Minimax Particle Filtering for Tracking a Highly Maneuvering Target

Jaechan Lim, Hun-Seok Kim, and Hyung-Min Park

Abstract

In this paper, we propose a new framework of particle filtering that adopts the minimax strategy. In the approach, we minimize a maximized risk, and the process of the risk-maximization is reflected when computing the weights of particles. This scheme results in the significantly reduced variance of the weights of particles that enables the robustness against the degeneracy problem, and we can obtain improved quality of particles. The proposed approach is robust against environmentally adverse scenarios, particularly when the state of a target is highly maneuvering. Further, we can reduce the computational complexity by avoiding the computation of a complex joint probability density function. We investigate the new method by comparing its performance to that of standard particle filtering and verify its effectiveness through experiments. The employed strategy can be adopted for any other variants of particle filtering to enhance tracking performance.

Index Terms

Bearing, minimax, particle filtering, range, risk, target tracking.

I. Introduction

Conventional adaptive filters such as the adaptive Kalman filter can be applied to maneuvering target tracking [1]. In this adaptive filter, two additional schemes exist beyond the standard Kalman filtering, i.e., maneuvering detection and adjusting the state noise variance. This adaptive filter can be applied to the problems of tracking a maneuvering target by white-noise acceleration models. More recently, the interactive multiple model (IMM) EKF was proposed for tracking maneuvering targets where the state model varies based on multiple constant turn models. IMM-EKF has been successfully applied for tracking

J. Lim and H. Kim are with the Department of Electrical Engineering and Computer Science, University of Michigan, Ann Arbor, 48109 U.S. H.-M. Park (corresponding author, e-mail: hpark@sogang.co.kr) is with the Department of Electronic Engineering, Sogang University, Seoul, 04107, Republic of Korea. J. Lim is also with the Department of Electronic Engineering, Sogang University.

a maneuvering target across various problems. Particle filtering (PF) was applied in the form of IMM that outperformed conventional IMM-EKF, as shown in [2], [3]. PF was applied for solving this highly nonlinear-estimation-problem where the particles are used to approximate the probability density function because we cannot compute the expected state with respect to the posterior function in a closed-form.

PF has demonstrated powerful tracking performance in various dynamic state estimation problems, particularly when the state system and measurement functions are nonlinear functions with respect to the "state." Since its initial implementations in the 1990s, PF has become even more powerful owing to significant advancements in computing processors that enabled practical implementations in various problems [4][5]. Further, various variants of PF have been proposed since its initial proposal, such as auxiliary PF (APF) [6], regularized PF (RPF) [7], Kullback-Leibler divergence PF (KLDPF) [8][9][10], Gaussian PF (GPF) [11][12], and cost-reference PF (CRPF) [13][14][15]. The APF algorithm is the same as that of sequential importance resampling PF (SIRPF) until the resampling process; thereafter, we go back to the previous time step and propagate the particles again based on resampled particles. Standard PF (SPF) undergoes its inherent defect of particle impoverishment, and RPF was particularly modified from SPF to overcome the problem. The primary feature of KLDPF is that the number of employed particles is optimized adaptively based on a predefined error bound at every time step. GPF comprises a simple algorithm with excellent performance that does not require resampling, which makes GPF robust against particle impoverishment phenomenon that results from the resampling process. CRPF is applied with unknown noise statistical information, and is robust against particle impoverishment because the employed proposal density is based on a Gaussian function as in GPF.

Theoretically, PF can show optimal performance with infinitely many particles in nonlinear problems, and outperforms various sub-optimal approaches such as the extended Kalman filter and Kalman variants, with a reasonable number of particles. Nevertheless, occasionally, we are not able to obtain satisfactory results by PF when the time-varying target state varies drastically and highly maneuvers. One crucial factor for the non-ideal performance of PF is that degeneracy problem; that is, after a few iterations, we have only one particle that has meaningful weight while all the other particles have almost zeros weights, and the variance of the weights only increases over time that eventually results in unsatisfactory performance of PF [16]. To get over with the degeneracy problem, the resampling process is adopted that regenerate high-quality particles more often; nonetheless, we also have a side effect of particle impoverishment by resampling that we may have all the same particles within a few iterations, particularly when we have very small state noise. Therefore, the variance of the weights of particles is crucial to obtain the successful performance of PF approaches. To this end, we adopt a minimax strategy by which we can obtain significantly reduced the variance of the weights of particles that eventually results in robustness against maneuvering target and improved tracking performance of PF approaches. In this framework, we maximize a predefined risk function on

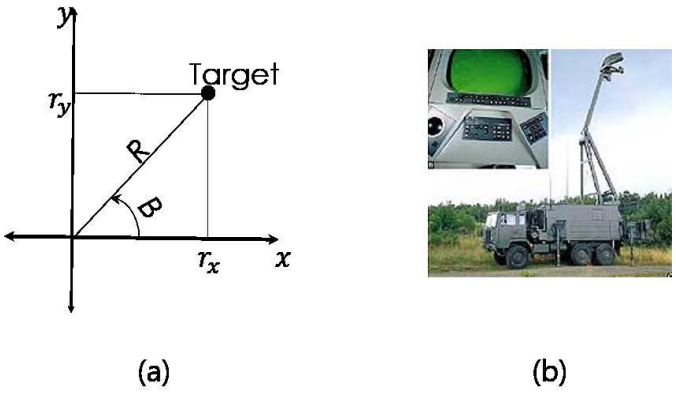

Fig. 1. Target is tracked based on range R and bearing B in radar.

the condition that the risk is bounded over time; subsequently, we obtain the estimator that minimizes the maximized risk function. Therefore, the bounded maximum risk is minimized in this strategy to avoid the worst-case divergence from true trajectories and provides more robust performance. In this strategy, the focus is directed to avoiding large errors rather than merely minimizing errors in the problem where large errors exist due to large variations in the state. To accomplish this goal, we follow the same criterion of minimum mean square error (MMSE) while using the possible maximum MSE as a risk function to be minimized.

In this paper, we propose a new algorithm of minimax-PF (MPF), especially for tracking problems where a target state is highly maneuvering. We show the outperforming results of the proposed MPF compared to standard PF. Further, we employ the minimax strategy to IMM-PF and show its outperforming result over conventional IMM-EKF and IMM-PF. The proposed approach can be adopted for any variants of PF to improve their tracking performances as shown in the experiments.

This paper is organized as follows. In Section II, we describe the problem formulation. In Section III, we describe the proposed MPF. In Section IV, we assess the performance of the proposed MPF compared to non-minimax particle filers; besides, we apply the minimax strategy to IMM-PF and compare the performances of IMM-EKF, IMM-PF, and IMM-MPF. Finally, we conclude and provide remarks in the last section.

II. Problem Formulation

In this problem, we track the location and velocity of a single target in a two-dimensional space where a target is moving with random acceleration based on range and bearing measurements. This problem is of interest in various applications such as radar systems and is a paradigm for target tracking problems. We estimate the state of the target based on observations measured at the origin of the coordinate system, as shown in Fig. 1(a). The moving direction of the target is subject to the

acceleration that is determined by the process noise in the state equation. We denote the state and measurement by $\boldsymbol{\theta}$ and $\boldsymbol{z}$, respectively, and the state equation is expressed as follows [17][18][19]:

$$\underbrace{\begin{bmatrix} r_{x,k} \\ r_{y,k} \\ v_{x,k} \\ v_{y,k} \end{bmatrix}}_{\boldsymbol{\theta}_k} = \underbrace{\begin{bmatrix} 1 & 0 & T & 0 \\ 0 & 1 & 0 & T \\ 0 & 0 & 1 & 0 \\ 0 & 0 & 0 & 1 \end{bmatrix}}_{\boldsymbol{A}_1} \underbrace{\begin{bmatrix} r_{x,k-1} \\ r_{y,k-1} \\ v_{x,k-1} \\ v_{y,k-1} \end{bmatrix}}_{\boldsymbol{\theta}_{k-1}} + \boldsymbol{A}_2 \boldsymbol{u}_k, \tag{1}$$

where

$$\boldsymbol{A}_2 = \begin{bmatrix} \frac{T^2}{2} & 0 \\ 0 & \frac{T^2}{2} \\ T & 0 \\ 0 & T \end{bmatrix}, \quad \boldsymbol{u}_k = \begin{bmatrix} u_{x,k} \\ u_{y,k} \end{bmatrix}, \tag{2}$$

r, v, u, and (x, y) denote the location, velocity, acceleration, and coordinates, respectively. T is the sampling period, and k is the discrete-time index. Therefore, the time-varying state is composed of four elements, i.e., 2-D location and 2-D velocity. The state of the location and the velocity are subjected to a random process of $\boldsymbol{u}_k$. The range and bearing compose the measurement equation, which is highly nonlinear, and described as follows:

$$\boldsymbol{z}_k = \boldsymbol{f}\left(\boldsymbol{\theta}_k\right) + \boldsymbol{\epsilon}_k = \left[R_k \; B_k\right]^\top + \boldsymbol{\epsilon}_k, \tag{3}$$

where

$$\boldsymbol{z}_k = \left[z_{1,k} \; z_{2,k}\right]^\top, \quad \boldsymbol{f}\left(\boldsymbol{\theta}_k\right) = \left[f_1\left(\boldsymbol{\theta}_k\right) \; f_2\left(\boldsymbol{\theta}_k\right)\right]^\top, \tag{4}$$

the range

$$z_{1,k} = z_{R,k} = R_k + \epsilon_{R,k} = \sqrt{r_{x,k}^2 + r_{y,k}^2} + \epsilon_{R,k}, \tag{5}$$

the bearing

$$z_{2,k} = z_{B,k} = B_k + \epsilon_{B,k} = \arctan 2\left(r_{y,k}, r_{x,k}\right) + \epsilon_{B,k}, \tag{6}$$

and the measurement noise $\boldsymbol{\epsilon}_k = \left[\epsilon_{R,k} \; \epsilon_{B,k}\right]^\top$. $\arctan 2\left(r_{y,k}, r_{x,k}\right)$ denotes the four-quadrant inverse tangent that acts on $r_{y,k}$ and $r_{x,k}$ element-wise to return B_k. We assume that a measurement noise ϵ_i for the measurement $z_{i,k}$ follows a zero-mean white Gaussian:

$$\epsilon_{i,k} \sim \mathcal{N}\left(0, \sigma_{i,k}^2\right) \quad \text{for} \;\; i = 1, \ldots, M, \tag{7}$$

where M is the total number of employed measurements. In this case, the likelihood function with respect to only $z_{i,k}$ becomes

$$p(z_{i,k}|\boldsymbol{\theta}_k) = \frac{1}{\sqrt{2\pi\sigma_{i,k}^2}} \exp\left\{-\frac{\left[z_{i,k} - f_i\left(\boldsymbol{\theta}_k\right)\right]^2}{2\sigma_{i,k}^2}\right\}. \tag{8}$$

III. Proposed Approach

A. Minimax approach

In game theory, a minimax approach is employed as a solution for zero-sum-game problems [20][21]. We model the tracking problem as a game where one player is the estimator that tries to obtain the accurate values of the time-varying state whereas the other player is the environment that adds the noise to the state and measurements to disturb the other player estimating the state. In this approach, the cost function is designed based on the strategy that the probability of the maximum-expected-point-loss is minimized regardless of the strategy of the opponent. Therefore, the expected point-loss becomes the risk that is maximized before the minimization in the minimax strategy. The minimax approach minimizes its maximal risk among all estimators, which can be described as follows:

$$\inf_{\hat{\boldsymbol{\theta}}_k} \sup_{\boldsymbol{\epsilon}_k} \mathcal{R}_k\left(\boldsymbol{\theta}_k, \hat{\boldsymbol{\theta}}_k\right), \tag{9}$$

where "$\inf$," "$\sup$," and $\mathcal{R}$ denote "infimum," "supremum," and risk, respectively.

B. Minimax particle filtering (MPF)

In the minimum mean square error (MMSE) criterion of Bayesian estimation, the following mean square error is defined as the risk function to be minimized:

$$\int \left(\boldsymbol{\theta}_k - \hat{\boldsymbol{\theta}}_k^{\text{MMSE}}\right)^2 p(\boldsymbol{\theta}_{0:k}|\boldsymbol{z}_{1:k}) d\boldsymbol{\theta}_k \tag{10}$$

to obtain the following MMSE:

$$\hat{\boldsymbol{\theta}}_k^{\text{MMSE}} = \int \boldsymbol{\theta}_k p(\boldsymbol{\theta}_{0:k}|\boldsymbol{z}_{1:k}) d\boldsymbol{\theta}_k, \tag{11}$$

where the square error, $\left(\boldsymbol{\theta}_k - \hat{\boldsymbol{\theta}}_k^{\text{MMSE}}\right)^2$ is defined as the cost function in this MMSE estimator. Similarly, in PF,

$$\mathcal{R}_k^{\text{PF}} = \sum_{j_p=1}^{N} \left[\left(\boldsymbol{\theta}_k^{j_p} - \hat{\boldsymbol{\theta}}_k^{\text{PF}}\right)^2 \omega_k^{j_p}\right], \text{ where } \sum_{j_p=1}^{N} \omega_k^{j_p} = 1 \tag{12}$$

is the risk function that we minimize, where N is the number of employed particles, j_p is the particle index, $\omega_k^{j_p}$ is the weight of the particle j_p at time step k, and $\boldsymbol{\theta}_k^{j_p}$ is the particle with the index j_p; therefore, we obtain

$$\hat{\boldsymbol{\theta}}_k^{\text{PF}} = \sum_{j_p=1}^{N} \omega_k^{j_p} \boldsymbol{\theta}_k^{j_p}, \tag{13}$$

because

$$\frac{\partial \mathcal{R}_k^{\text{PF}}}{\partial \hat{\boldsymbol{\theta}}_k^{\text{PF}}} = -2\sum_{j_p=1}^{N} \boldsymbol{\theta}_k^{j_p}\omega_k^{j_p} + 2\hat{\boldsymbol{\theta}}_k^{\text{PF}} \sum_{j_p=1}^{N} \omega_k^{j_p}, \tag{14}$$

and (13) makes (14) zero.

To formulate the minimax strategy for PF, from (12), we describe a new risk function with respect to each particle as follows:

$$\mathcal{R}_k^{\text{MPF}} = \sum_{j_p=1}^{N} \mathcal{G}\left(\mathcal{R}_k^{\text{MPF},j_p}\right) = \sum_{j_p=1}^{N} \left[\left(\boldsymbol{\theta}_k^{j_p} - \hat{\boldsymbol{\theta}}_k^{\text{MPF}}\right)^2 \omega_k^{j_p}\right]. \tag{15}$$

In the proposed minimax-PF, we adopt a minimax strategy to the computations of the weights of particles. In particular, we select only one measurement that may incur the highest risk. That is, for M measurements, we use only use one measurement that provides the minimum weight rather than the maximum weight. Therefore, to apply this approach, multiple measurements are required otherwise the approach becomes identical to that of regular PF.

According to (15), only $\omega_k^{j_p}$ is the factor that affects the magnitude of the risk, and the weight can be associated with a measurement as follows:

$$\omega_k^{j_p} \in \left\{\omega_{1,k}^{j_p}, \omega_{2,k}^{j_p}, \ldots, \omega_{M,k}^{j_p}\right\}, \tag{16}$$

where, for example, $\omega_{1,k}^{j_p}$ is the weight of the particle $\boldsymbol{\theta}_k^{j_p}$ computed based on only the measurement $z_{1,k}$. The argument i is determined with respect to each particle. Therefore, in minimax-PF, we maximize the risk with respect to each particle by associating the minimum weight to a particle among M weights. Subsequently, we maximize the following total risk:

$$\mathcal{R}_k^{\text{MPF,Max}} = \sum_{j_p=1}^{N} \left[\left(\boldsymbol{\theta}_k^{j_p} - \hat{\boldsymbol{\theta}}_k^{\text{MPF}}\right)^2 \omega_{i_p,k}^{j_p}\right], \tag{17}$$

where the association between the measurement index i_p and the particle j_p is determined by

$$i_p = \underset{i\in\{1,\ldots,M\}}{\operatorname{argmin}}\ \omega_{i,k}^{j_p}, \tag{18}$$

and the estimate of MPF at time step k:

$$\hat{\boldsymbol{\theta}}_k^{\text{MPF}} = \sum_{j_p=1}^{N} \omega_{i_p,k}^{j_p}\boldsymbol{\theta}_k^{j_p}. \tag{19}$$

At every time step, for the computation of the weight of every single particle, we may select a different single measurement that devalues the particle as low as possible.

The MPF algorithm is summarized in Table I where only the boldfaced steps, i.e., $(b) \sim (d)$, of computing the weights of particles are different from those of a standard PF. Applying the proposed minimax strategy to any variants of PF is straightforward because it only requires modifying the step of computing the weights of particles.

TABLE I

ALGORITHM OF MINIMAX-PF FOR SIRPF. ONLY THE STEPS, WHICH ARE BOLDFACED, I.E., $(b) \sim (d)$, OF COMPUTING THE WEIGHTS OF PARTICLES ARE DIFFERENT FROM THOSE OF SPF.

- **Initialization**

  `for` $j_p = 1, \ldots, N$

  Particles are generated: $\boldsymbol{\theta}_0^{j_p} \sim p\left(\boldsymbol{\theta}_0\right)$, and assign weights: $\omega_0^{j_p} = 1/N$.

  `end`

- **Recursive update**

  `for` $k = 1, \ldots, K$(total time steps),

  `for` $j_p = 1, \ldots, N$,

  (a) Generate particles from a proposal density $q(\cdot)$: $\boldsymbol{\theta}_k^{j_p} \sim q\left(\boldsymbol{\theta}_k | \boldsymbol{\theta}_{k-1}^{j_p}, \boldsymbol{z}_k\right)$.

  (**b**) Compute the weights with respect to each measurement: $\omega_{i,k}^{j_p} = p(z_{i,k}|\boldsymbol{\theta}_k^{j_p})$ for $i = 1, \ldots, M$

  assuming we employ prior density, $q\left(\boldsymbol{\theta}_k | \boldsymbol{\theta}_{k-1}^{j_p}, \boldsymbol{z}_k\right) = p\left(\boldsymbol{\theta}_k | \boldsymbol{\theta}_{k-1}^{j_p}\right)$, as the proposal density.

  (**c**) Normalize the weights with respect to each measurement: $\bar{\omega}_{i,k}^{j_p} = \frac{\omega_{i,k}^{j_p}}{\sum_{j_p=1}^{N} \omega_{i,k}^{j_p}}$ for $i = 1, \ldots, M$.

  (**d**) Select the minimum weight among M weights for each particle:

  $$\omega_k^{j_p} = \bar{\omega}_{i_p,k}^{j_p}, \quad \text{where} \quad i_p = \underset{i \in \{1,\ldots,M\}}{\operatorname{argmin}} \bar{\omega}_{i,k}^{j_p}.$$

  `end`

  (e) Normalize the weights: $\bar{\omega}_k^{j_p} = \frac{\omega_k^{j_p}}{\sum_{j_p=1}^{N} \omega_k^{j_p}}$.

  (f) Compute the estimate: $\hat{\boldsymbol{\theta}}_k^{\text{MPF}} = \sum_{j_p=1}^{N} \bar{\omega}_k^{j_p} \boldsymbol{\theta}_k^{j_p}$.

  (g) Resample the particles [16].

  `end`

IV. PERFORMANCE ASSESSMENT

In this section, we assess the performance of the proposed minimax-PFs by comparing to that of regular PFs. We consider SIRPF first for a regular PF. Regarding the state noises, we first specify a parameter ξ and randomly generate a noise variance to be "$\xi \cdot \mathcal{U}(0,1)$," where $\mathcal{U}(0,1)$ is the standard uniform distribution. Subsequently, random noise is generated by a Gaussian distribution that has zero mean with the generated variance of $\xi \cdot \mathcal{U}(0,1)$. We performed experiments with two kinds of ξ in terms of magnitude to represent low and high maneuvering targets, respectively. We denote scenarios by S_S and S_L for small and large values of ξ, respectively. Fig. 2 shows an illustrative example of two trajectories of a target where two significantly different magnitudes of ξ are employed. With $\xi = 10$ for the state noise, the trajectory of the target labeled as T-1 shows highly maneuvering. On the contrary, a run with $\xi = 0.1$ results in the trajectory labeled as T-2 that shows significantly less maneuvering compared to T-1 during the same elapsed time.

For the measurement noises, we use ζ that plays the same role as ξ of the state noise. We have two ζs for range and

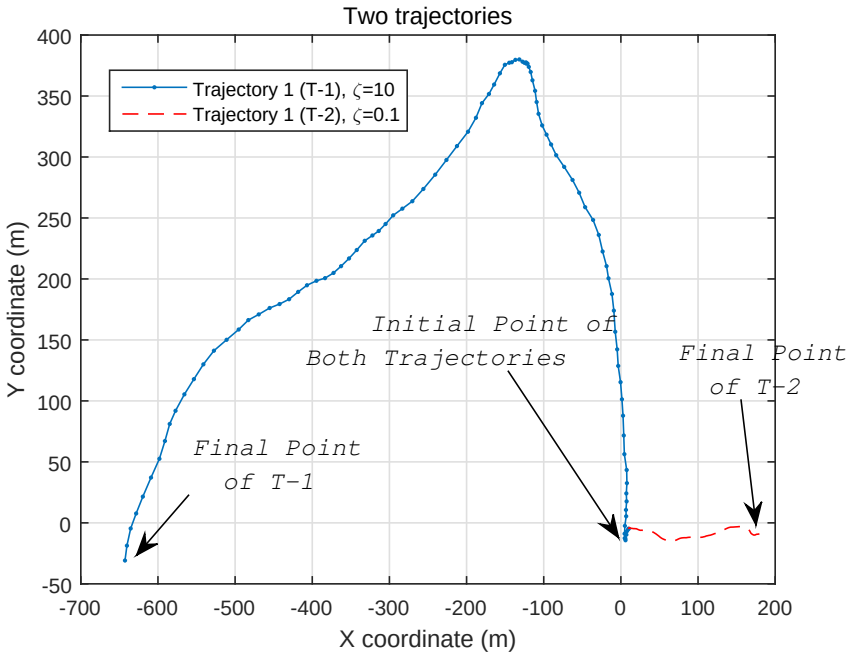

Fig. 2. An illustrative example of two trajectories of a target with $\xi = 0.1$ and 10 for the state noise during the same elapsed time. It is highly maneuvering with $\xi = 10$, i.e. T-1.

bearing measurements, i.e. ζ_R and ζ_B, respectively. We select $\xi = 10^{-3}$, $\zeta_R = 10^{-4}$, and $\zeta_B = 10^{-5}$ for S_S and $\xi = 1$, $\zeta_R = 5 \times 10^{-3}$, and $\zeta_B = 5 \times 10^{-4}$ for S_L The number of total time steps $K = 100$. We performed 500 experiments to obtain the mean square error (MSE) of distance (MSED) and mean distance error (MDE) for each location over time. The initial state is generated with a known variance.

The MDE and MSED of SPF, MPF, and Cramér-Rao lower bound (CRLB) are compared in Fig. 3. Figs. 3(a) and 3(b) show the results under S_S (ξ=0.1). Figs. 3(a) and 3(b) show that the performance of SPF and MPF is similar in this low maneuvering scenario while MPF shows marginally better performance than PF. The result with $\xi = 1$ is shown in Figs. 3(c) and 3(d) where we have significantly maneuvering trajectories, and MPF shows better performance than PF.

Based on (12), we computed the risk function for both PF frameworks, and the mean values over 500 runs are shown in Figs. 4-5. Fig. 4 shows that the risk by MPF is much higher than that of SPF. For comparison purposes, Fig. 5 shows the mean-risk of PF_{wmax} in addition to those of MPF and SPF. In PF_{wmax} framework, the minimum risk is adopted for each particle as opposed to the case of MPF. The resulting mean-risk of PF_{wmax} is not bounded and it diverges significantly such that we cannot perform a minimization to obtain an estimate. Although we did not show results, the estimation performance of PF_{wmax} is unduly poor, which is not acceptable. In the following subsections, we assess the performance of the minimax versions of PF approaches for other variants, such as APF, RPF, and KLDPF.

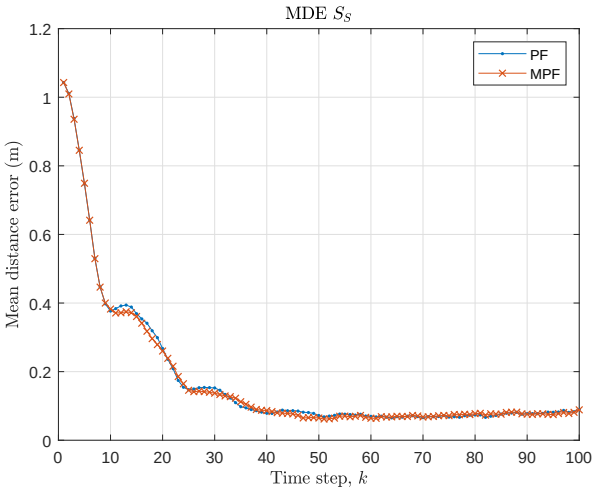

(a) Mean distance error with $\xi = 0.1$.

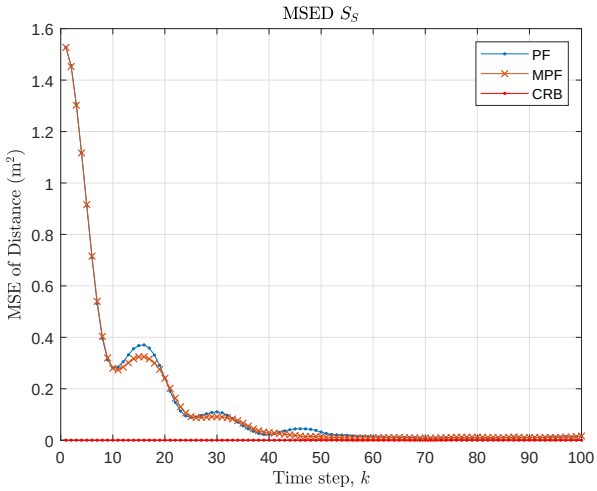

(b) MSE of distance with $\xi = 0.1$.

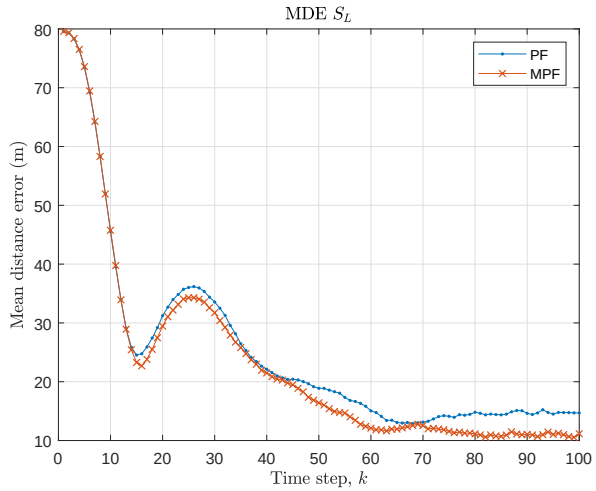

(c) Mean distance error with $\xi = 1$.

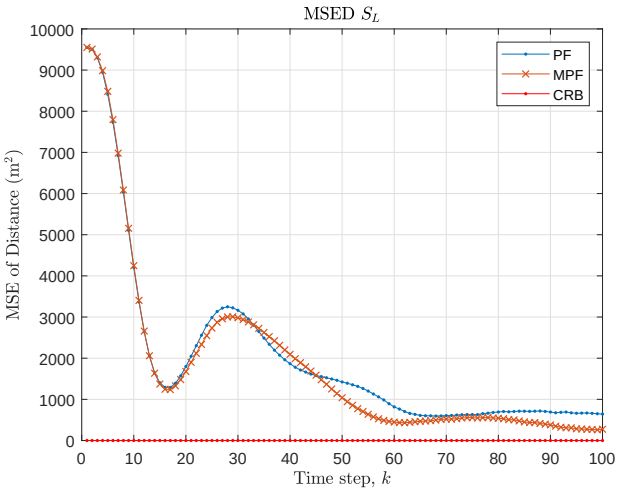

(d) MSE of distance with $\xi = 1$.

Fig. 3. Performance comparison between SIRPF and MPF. Trajectories manifest significant maneuvering when $\xi = 1$. 500 runs were performed with 500 particles. Comparison with Cramér-Rao lower bound (CRLB) was performed, as derived in the appendix.

A. Auxiliary Particle Filter

APF was initially introduced in [22] as a variant of SIRPF. We adopted the algorithm based on [16]. In this variant, the algorithm is the same to SIRPF except for the resampling process. Specifically, APF returns to the previous time step after the resampling particles and then propagates the particles again for the next time step. We used $\xi = 10^{-3}$, $\zeta_R = 10^{-4}$, and $\zeta_B = 10^{-5}$ for S_S and $\xi = 10^{-2}$, $\zeta_R = 10^{-3}$, and $\zeta_B = 10^{-4}$ for S_L in the experiments.

The results are shown in Fig. 6 where MAPF outperforms APF even under the scenario of S_S.

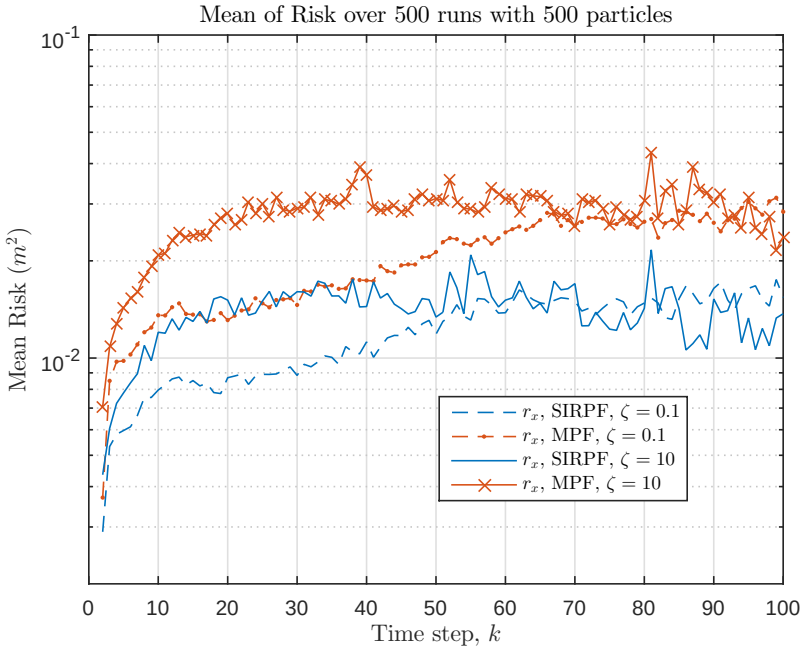

Fig. 4. Mean-risk over 500 runs with 500 particles in log-scale based on (12). Results regarding only r_x are shown, and those of the remaining elements are similar to those of r_x. Mean-risk for SIRPF and MPF for $\xi = 0.1$ and 10. The same values of $\xi_R = 0.1$ and $xi_B = 0.001$ are applied for both scenarios.

B. Regularized PF

In the regularized particle filtering (RPF), PF was modified to resolve the particle impoverishment problem [23]. RPF employs a kernel density that perturbs the state of a particle to achieve the diversity of the particle states. Specifically, the posterior density is approximated in RPF as follows:

$$p(\boldsymbol{\theta}_k|z_{1:k}) \approx \sum_{i=1}^{M} \omega_k^{j_p} \Gamma_\kappa \left(\boldsymbol{\theta}_k - \boldsymbol{\theta}_k^{j_p}\right) \tag{20}$$

where $\Gamma_\kappa(\boldsymbol{\theta}) = \frac{1}{\kappa^{n_{\boldsymbol{\theta}}}}\Gamma\left(\frac{\boldsymbol{\theta}}{\kappa}\right)$ is the rescaled kernel density for any kernel bandwidth $\kappa > 0$, and $n_{\boldsymbol{\theta}}$ is the dimension of the state parameter $\boldsymbol{\theta}$. The optimal choice of the kernel is the *Epanechnikov* kernel; however, it can be replaced by the Gaussian kernel [24]. Subsequently, the associated optimal bandwidth is

$$\kappa_{opt} = AN^{-\frac{1}{n_{\boldsymbol{\theta}}+4}}, \text{ where } A = \left(\frac{4}{n_{\boldsymbol{\theta}}+2}\right)^{\frac{1}{n_{\boldsymbol{\theta}}+4}}. \tag{21}$$

In this study, we use $n_{\boldsymbol{\theta}} = 4$ with $N = 500$ particles to perform experiments and compare the performances of RPF and minimax-RPF (MRPF). We used $\xi = 10^{-3}$, $\zeta_R = 10^{-4}$, and $\zeta_B = 10^{-5}$ for S_S and $\xi = 1$, $\zeta_R = 0.1$, and $\zeta_B = 10^{-2}$ for S_L in the experiments. The results are shown in Fig. 7, where MRPF outperforms RPF even under the scenario of S_S, as shown in Figs. 7(a) and 7(b). Under both scenarios, MRPF outperforms RPF.

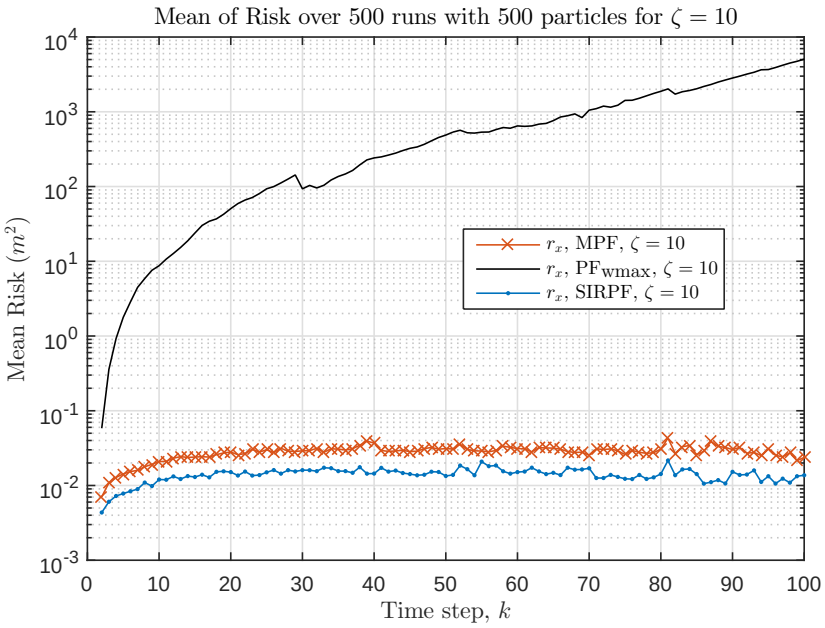

Fig. 5. Mean-risk over 500 runs with three measurements and 500 particles in log-scale based on (12). Results regarding only r_x are shown, and those of the remaining elements are similar to those of r_x. Mean-risk of PF$_{\text{wmax}}$ is not bounded and diverges over time steps where we use the maximum weight for particles in PF$_{\text{wmax}}$.

C. KLDPF

A primary feature of KLDPF is that the number of employed particles is optimized adaptively based on a predefined error bound at every time step [8]. While it may not show better performance than SPF, the number of employed particles is dynamically adjusted to reduce redundant particles and also unnecessary computations accordingly. We adopt the KLDPF algorithm introduced in [9] with an error bound of 0.01. The initial number of employed particles is 250 and the maximum number of particles is bounded by 500. The probability bound is 0.01; the bin size is $1/2 \times \sqrt{\boldsymbol{\delta}_{u_k}} \times 4$ as suggested in [9], where $1/2$ is from $A2$; $\delta_{\boldsymbol{u}_k}$ is the variance of the state noise with respect to v_x or v_y. Although KLDPF adaptively optimizes the number of particles at every time step, the algorithm inherently requires a higher computational cost than those of other PF variants.

We used $\xi = 10^{-3}$, $\zeta_R = 10^{-4}$, and $\zeta_B = 10^{-5}$ for S_S and $\xi = 10$, $\zeta_R = 0.1$, and $\zeta_B = 10^{-3}$ for S_L in the experiments. MKLDPF outperforms KLDPF in both scenarios as shown in Fig. 8. Fig. 9 shows the mean number of the employed particles for the scenarios of highly maneuvering target tracking, where MKLDPF requires marginally more number of particles than that required by regular KLDPF.

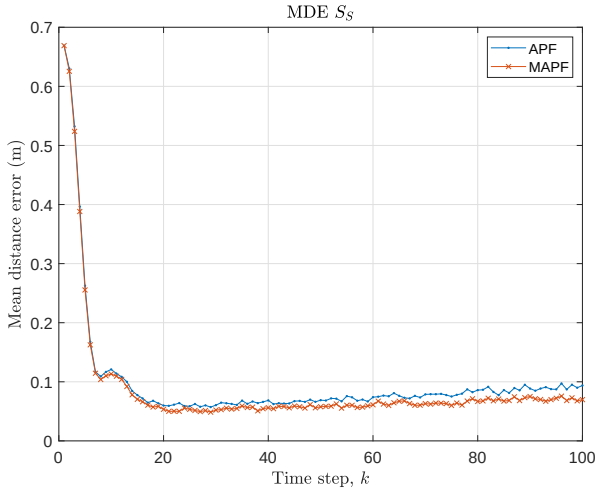

(a) Mean distance error with $\xi = 10^{-3}$.

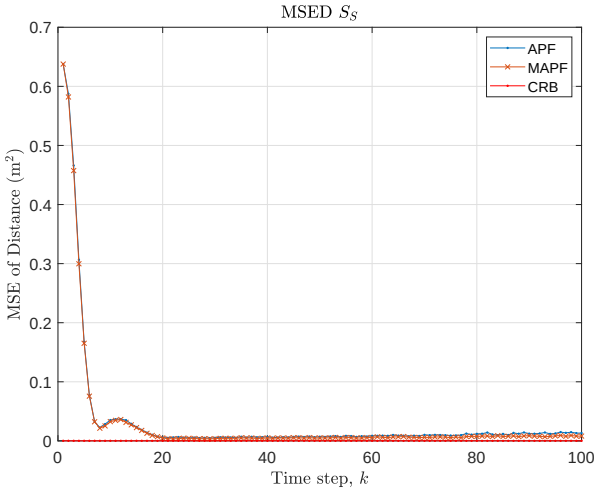

(b) MSE of distance with $\xi = 10^{-3}$.

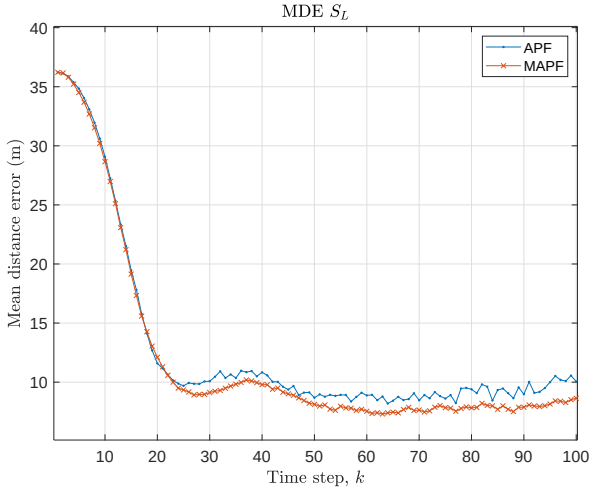

(c) Mean distance error with $\xi = 10^{-2}$.

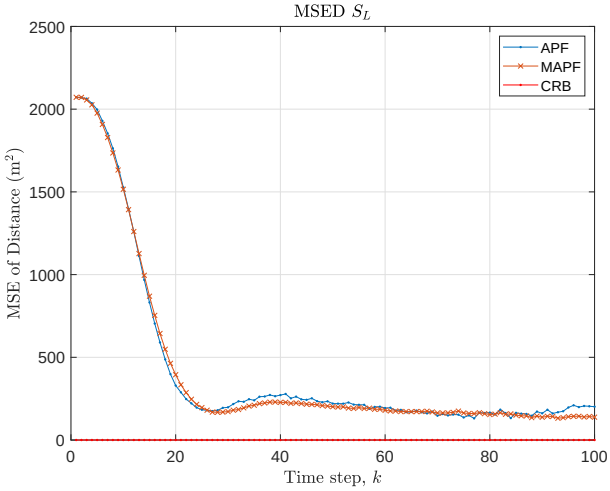

(d) MSE of distance with $\xi = 10^{-2}$.

Fig. 6. Performance comparison between APF and MAPF. 500 runs were performed with 500 particles.

D. Comparison with Interactive Multiple Model Filters

Finally, we adopt the minimax strategy to the interactive multiple model (IMM) particle filtering. A conventional IMM-extended Kalman filter (EKF) evaluation is compared to the IMM-minimax-PF (IMM-MPF) approach in this experiment. We refer to [25] and [3] for IMM-EKF and IMM-PF, respectively. The results are shown in Fig. 10 where IMM-MPF outperforms IMM-PF and IMM-EKF. We used $\xi = 0.1$, $\zeta_R = 10^{-2}$, and $\zeta_B = 10^{-2}$ in the experiments.

E. Discussion

The proposed MPF was derived based on the same criterion as a Bayesian method that minimizes MSE, except for the main difference that the proposed approach adopts the maximum risk among various options of risk functions. Unlike conventional

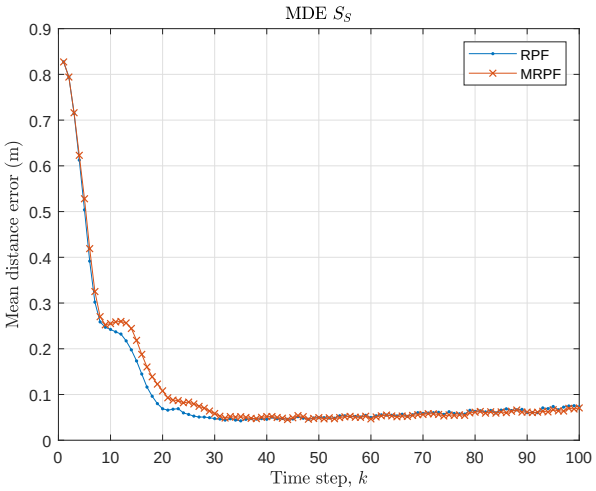

(a) Mean distance error with $\xi = 0.1$.

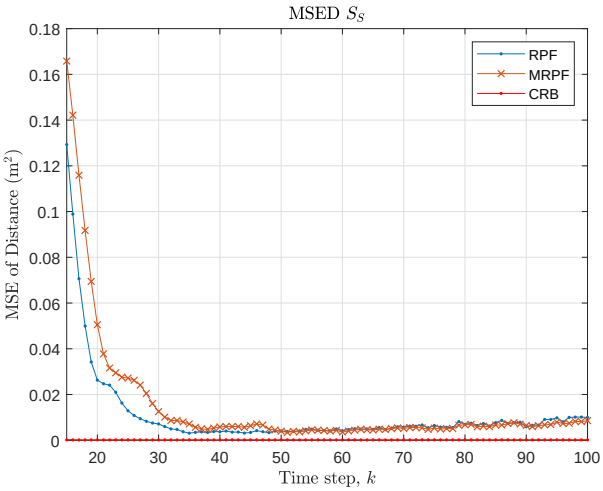

(b) MSE of distance with $\xi = 0.1$.

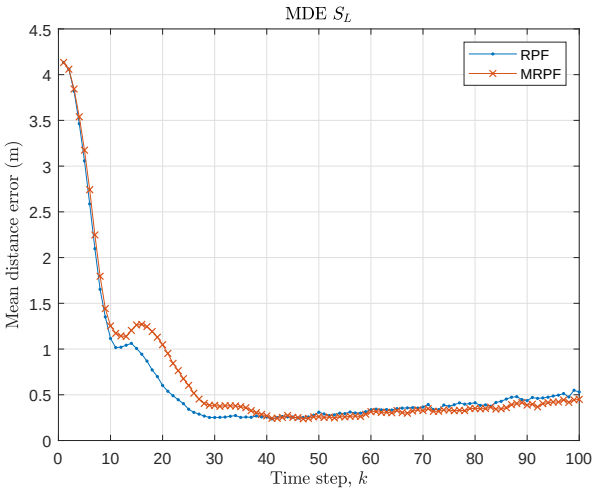

(c) Mean distance error with $\xi = 1$.

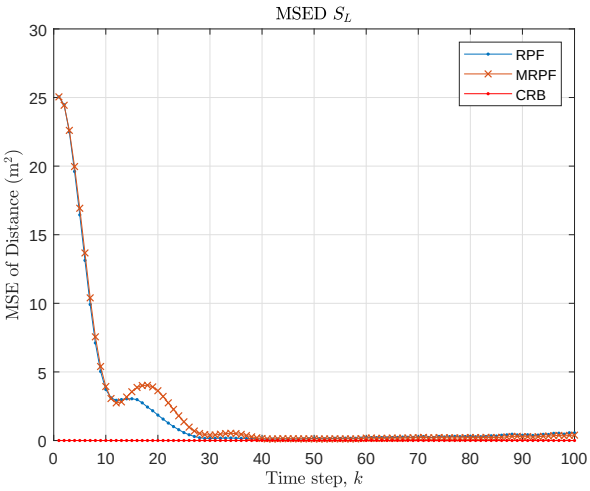

(d) MSE of distance with $\xi = 1$.

Fig. 7. Performance comparison between RPF and MRPF. 500 runs were performed with 500 particles.

Bayesian-MMSE-PF approaches where the weight of each particle is computed based on joint probability density (i.e., usually multiplication of likelihood functions of all measurements assuming white Gaussian noise), the proposed minimax approach selects the minimum weight based on a single measurement for each particle. We obtain the estimate based on these weights that are selected to minimize the maximized risk. This strategy enables the significantly reduced variance of the weights of particles. We can obtain improved quality of particles by the reduced variance, and eventually improve the tracking performance. Therefore, the proposed minimax strategy makes the filter robust against the degeneracy problem of standard PF approaches.

The proposed approach is computationally efficient because it does not require computing a joint probability for the weight of a particle. Computation of joint probability based on multiple measurements typically undergoes substantial computational load owing to additional multiplications.

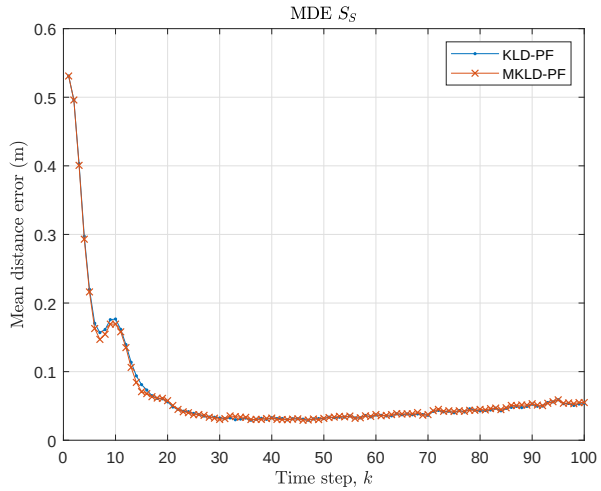

(a) Mean distance error with $\xi = 10^{-3}$.

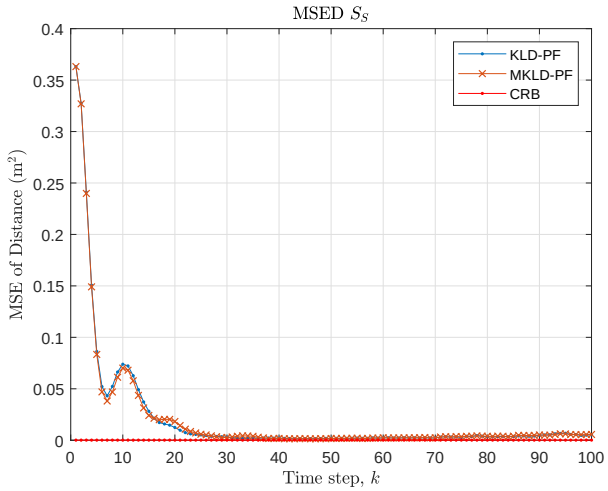

(b) MSE of distance with $\xi = 10^{-3}$.

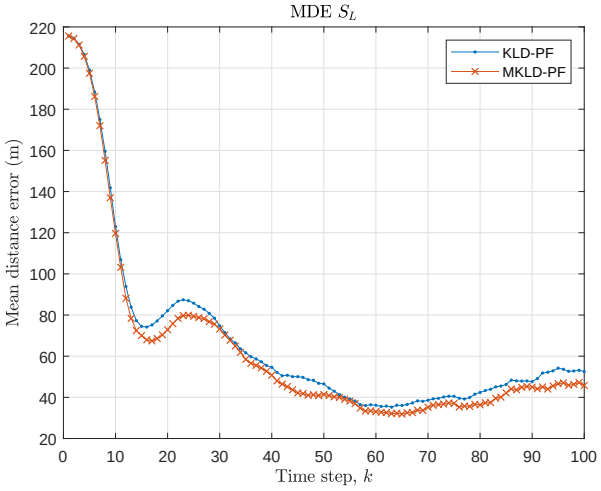

(c) Mean distance error with $\xi = 10$.

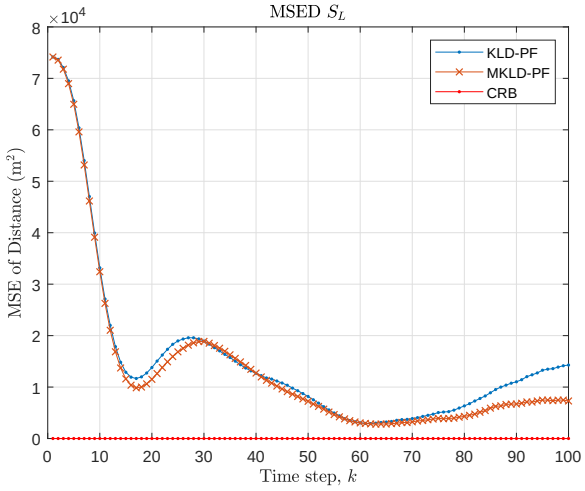

(d) MSE of distance with $\xi = 10$.

Fig. 8. Performance comparison between KLDPF and MKLDPF. The initial number of particles is 200 with a maximum of 500 particles.

We compared the performances of all minimax-PF approaches together. The results are shown in Figs. 11 and 12 under S_S and S_L scenarios, respectively. We used $\xi = 10^{-3}$, $\zeta_R = 10^{-4}$, and $\zeta_B = 10^{-5}$ for S_S and $\xi = 1$, $\zeta_R = 0.1$, and $\zeta_B = 10^{-2}$ for S_L in the experiments. All minimax PFs show similar performance under the scenario of S_S while both MAPF and MRPF show similarly better performance compared to the other two approaches under the scenario of S_L.

We also computed the mean-variance of the weights of particles during the previous experiments for all minimax-PFs. Figs. 13 show the mean variances of each minimax-PF under both scenarios of S_S and S_L. The results show that we can obtain significantly reduced variances by minimax-PFs compared to regular PFs regardless of the scenarios.

We obtained normalized estimation error squared (NEES) and average NEES (ANEES) for all particle filtering approaches concerning both regular and minimax versions. We used $\xi = 10^{-3}$, $\zeta_R = 10^{-4}$, and $\zeta_B = 10^{-5}$, which is close to the scenario

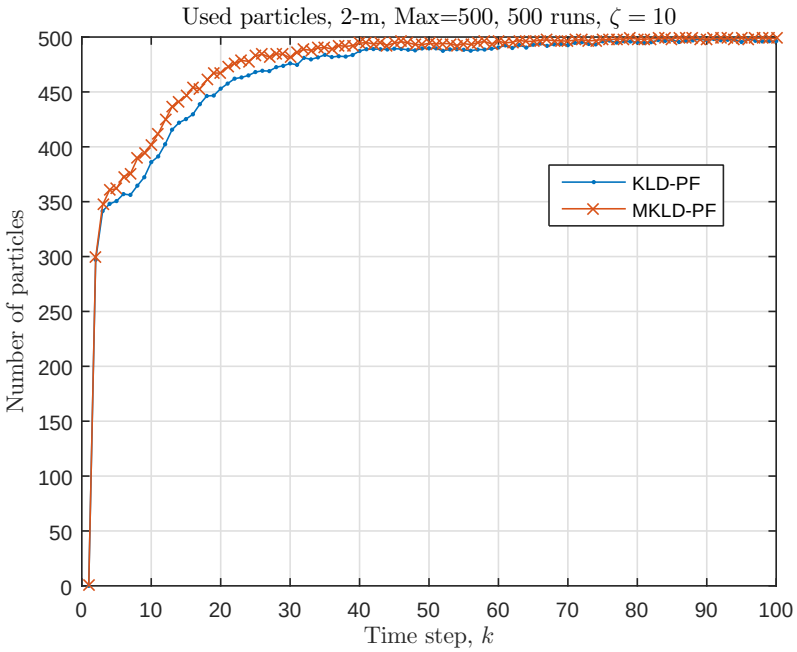

Fig. 9. The number of employed particles with 500 maximum particles in KLDPF, two measurements, and $\xi = 10$.

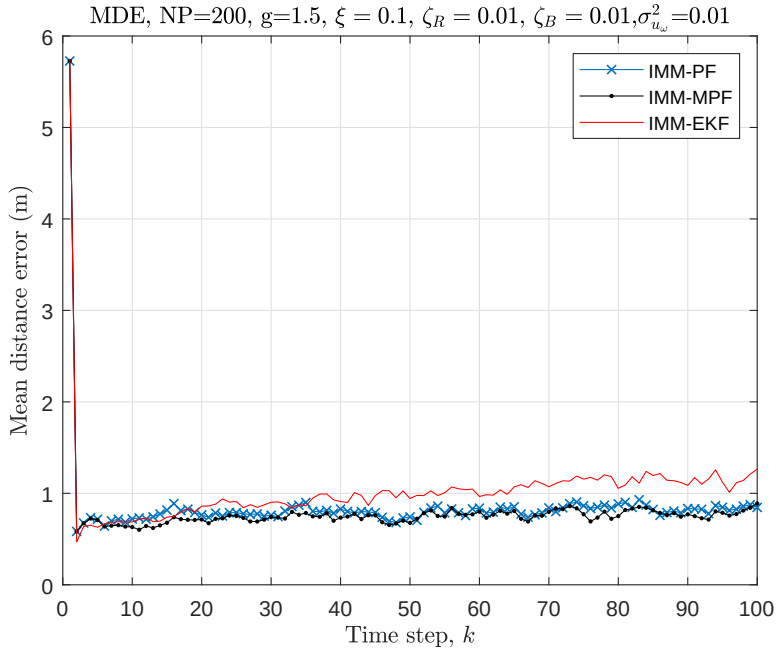

Fig. 10. Mean distance error comparison of IMM-EKF, IMM-PF, and IMM-MPF under S_S, where σ_{u_ω} is the noise variance of the turn rate.

of S_S in the experiments. Based on [26], NEES and ANEES are defined, respectively, as follows.

$$\chi_r = \left(\boldsymbol{\theta}_r - \hat{\boldsymbol{\theta}}_r\right)^\top P_r^{-1} \left(\boldsymbol{\theta}_r - \hat{\boldsymbol{\theta}}_r\right) \tag{22}$$

$$\bar{\chi}_r = \frac{1}{LR} \sum_{r=1}^{R} \chi_r, \tag{23}$$

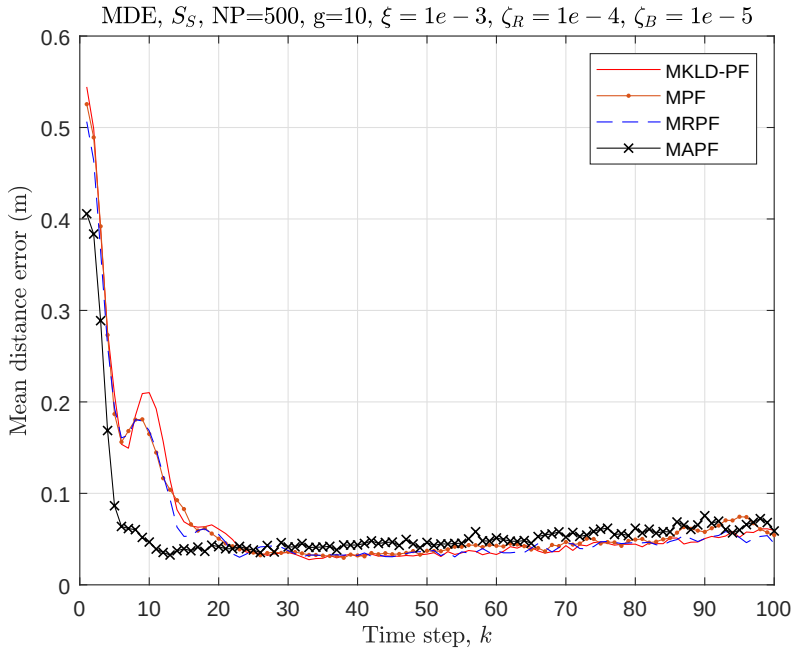

Fig. 11. Results of MDE for minimax approaches under S_S. All show similar performance.

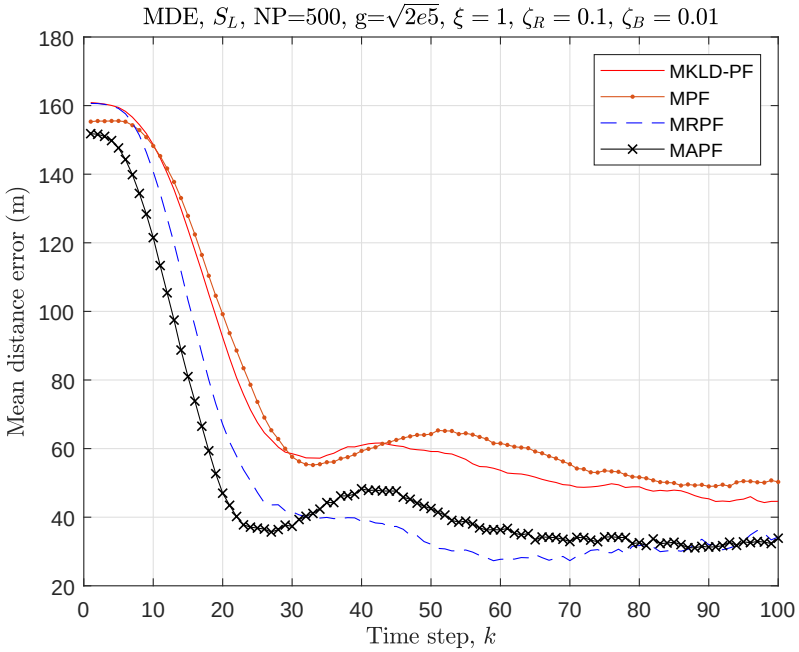

Fig. 12. Results of MDE for MPF approaches under S_L. MAPF and MRPF show similarly better performance than the other two.

where r is the index of a run, L is the dimension of the state $\boldsymbol{\theta}$, P is the estimator-provided error covariance, R is the number of runs, respectively. According to [26], ANEES is recommended for testing whether an estimator should be rejected as not credible or is optimistic or pessimistic. The closer to 1 the ANEES is, the more credible the estimator. If ANEES is much greater than 1, the actual estimation error is much larger than what the estimator believes (i.e., the estimator is unduly

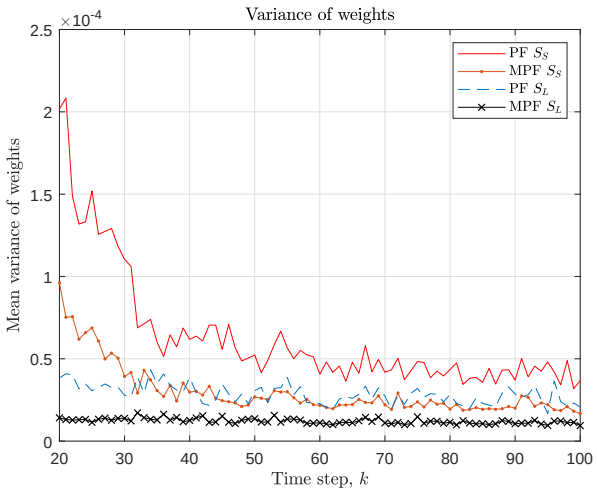

(a) Mean-variance: PF and MPF.

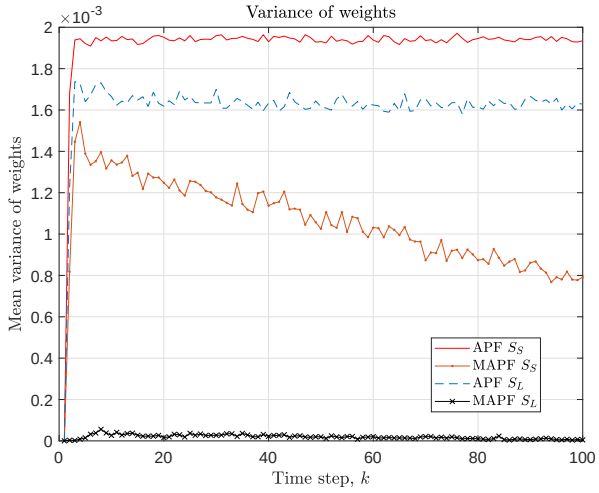

(b) Mean-variance: APF and MAPF.

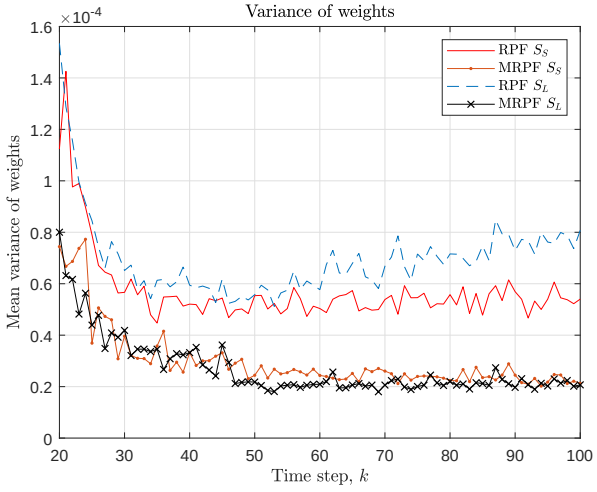

(c) Mean-variance: RPF and MRPF.

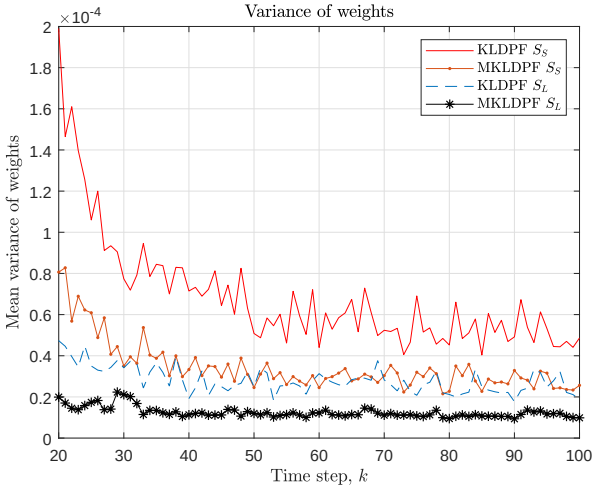

(d) Mean-variance: KLDPF and MKLDPF.

Fig. 13. Mean-variance of the weights of particles. The results are shown from at the time step 20 for PF, RPF, and KLDPF for clear visibility.

optimistic); if ANEES is much smaller than 1, the actual estimation error is much smaller than what the estimator believes (i.e., the estimator is unduly pessimistic). Fig. 14 shows the result of ANEES for four of all particle filtering methods concerning both regular and minimax versions. The results are under S_S and various sizes of variances of initial values. The ANEES depends on the noises and the magnitude of the variance of the initial values; however, most results show more or less around 1 with small noises that we applied in these 300 runs. In our case, $L = 4$. Most of the approaches are somewhat too pessimistic, i.e. the actual estimation error is much smaller than what the estimator believes.

V. Conclusion

In this paper, we proposed a new PF framework for highly maneuvering target tracking. The minimax strategy was adopted in this framework that results in the significantly reduced variance of the weights of particles and in robustness against

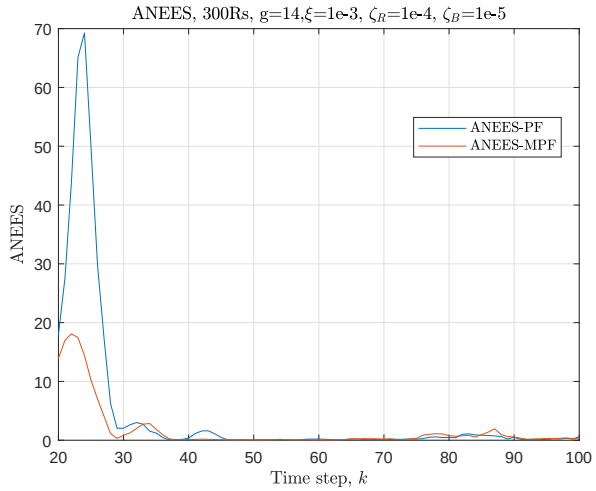

(a) ANEES for PF vs. MPF.

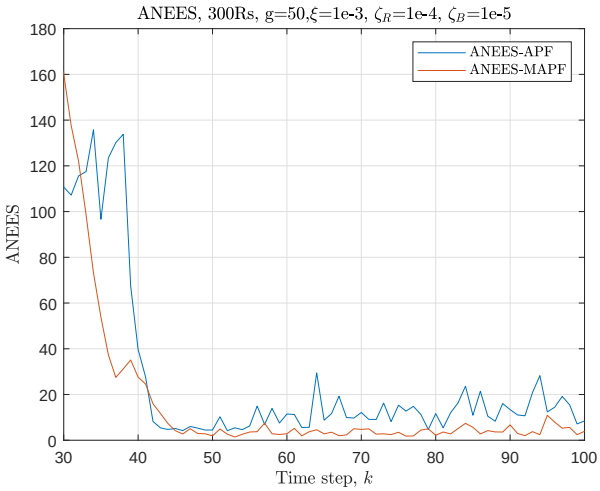

(b) ANEES for APF vs. MAPF

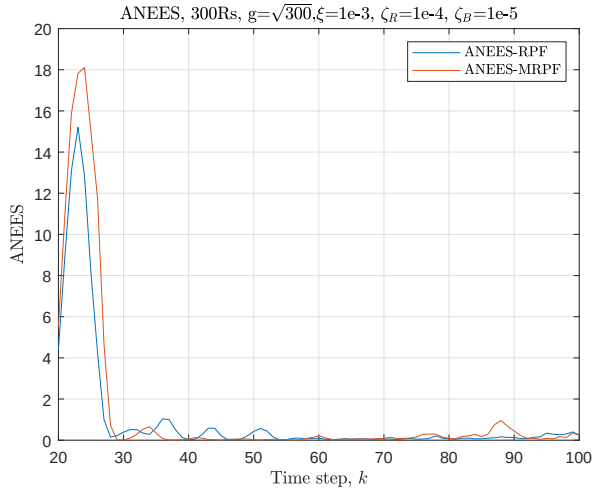

(c) ANEES for RPF vs. MRPF

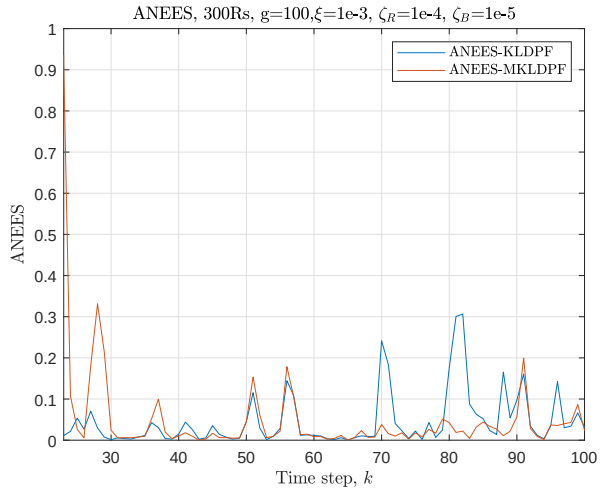

(d) ANEES for KLDPF vs. MKLDMPF

Fig. 14. ANEES with the scenario of S_S.

the degeneracy problem of regular PF approaches. The robustness made it possible to overcome the difficulty in tracking a highly maneuvering target where particularly the state noise variance is large. We verified the effectiveness of the proposed MPF by experiments in various scenarios, and showed that MPF outperforms non-minimax PF approaches. The proposed minimax strategy can be adopted for any other variants of PF provided that multiple measurements are available including sensor-networks-environment. The computational complexity in MPF was reduced because the computation of complex joint probability density function was avoided in the proposed algorithm. We further showed that the minimax strategy is effective in the form of IMM-PF, and minimax IMM-PF outperformed IMM-PF and conventional IMM-EKF.

APPENDIX

The variance of any unbiased estimate, $\hat{\boldsymbol{\theta}}$ is bounded as follows:

$$\mathsf{Var}(\hat{\boldsymbol{\theta}}_t) \geq \left[\mathbf{I}^{-1}(\boldsymbol{\theta})\right]_{tt}, \tag{24}$$

where $\mathbf{I}$ is the Fisher information matrix, $\boldsymbol{\theta}$ is a vector state, and t is the element index. When the measurement noise is Gaussian and the measurement is given by

$$\boldsymbol{z} \sim \mathcal{N}\left(f(\boldsymbol{\theta}), \boldsymbol{C_v}(\boldsymbol{\theta})\right), \tag{25}$$

we can obtain

$$[\mathbf{I}(\theta)]_{tl} = \left[\frac{\partial f(\boldsymbol{\theta})}{\partial \theta_t}\right]^{\top} \boldsymbol{C_v}^{-1}(\boldsymbol{\theta}) \left[\frac{\partial f(\boldsymbol{\theta})}{\partial \theta_l}\right] + \frac{1}{2}\mathrm{tr}\left[\left(\boldsymbol{C_v}^{-1}(\boldsymbol{\theta})\frac{\partial \boldsymbol{C_v}(\boldsymbol{\theta})}{\partial \theta_t}\boldsymbol{C_v}^{-1}(\boldsymbol{\theta})\frac{\partial \boldsymbol{C_v}(\boldsymbol{\theta})}{\partial \theta_l}\right)\right]. \tag{26}$$

For three measurements, $f(\boldsymbol{\theta}) = [f_1 \;\; f_2 \;\; f_3]^{\top} = [R \;\; B \;\; M]^{\top}$, and the covariance matrix $\mathbf{C}_{\epsilon}(\boldsymbol{\theta}) = diag\left(\sigma^2_{\epsilon_R}\; \sigma^2_{\epsilon_B}\; \sigma^2_{\epsilon_M}\right)$ where $diag\,(\cdot)$ denotes a diagonal matrix,

$$\sigma^2_{\epsilon_{f_i}} = {f_i}^2 \cdot 10^{\left(-\mathrm{SNR}_{z_1}/10\right)}, \tag{27}$$

where SNRz_1, SNRz_2, and SNRz_3 represent the SNRs for the corresponding measurements, and are computed as follows:

$$\mathrm{SNR}_{z_i} = 10\log_{10}\left[\frac{{f_i}^2}{\sigma^2_{\epsilon_{f_i}}(\boldsymbol{\theta})}\right]. \tag{28}$$

The Fisher information is a 4×4 matrix, and $[\mathbf{I}(\theta)]_{11}$ and $[\mathbf{I}(\theta)]_{22}$ are the corresponding elements for r_x and r_y, respectively. From (26),

$$[\mathbf{I}(\theta)]_{11} = R^{-4} \cdot \left[2r_x^2 + \frac{{r_x}^2}{10^{\left(-\mathrm{SNR}_{z_1}/10\right)}} + \frac{r_y^2 \cdot 10^{\left(\mathrm{SNR}_{z_2}/10\right)}}{\left[\arctan 2(r_y, r_x)\right]^2} + \frac{2r_y^2}{\left[\arctan 2(r_y, r_x)\right]^2}\right] + \frac{10^{\left(\mathrm{SNR}_{z_3}/10\right)}}{{r_x}^2} + \frac{2}{{r_x}^2}, \tag{29}$$

and

$$[\mathbf{I}(\theta)]_{22} = R^{-4} \cdot \left[2r_y^2 + \frac{{r_y}^2}{10^{\left(-\mathrm{SNR}_{z_1}/10\right)}} + \frac{r_x^2 \cdot 10^{\left(\mathrm{SNR}_{z_2}/10\right)}}{\left[\arctan\left(\frac{r_y}{r_x}\right)\right]^2} + \frac{2r_x^2}{\left[\arctan\left(\frac{r_y}{r_x}\right)\right]^2}\right] + \frac{10^{\left(\mathrm{SNR}_{z_3}/10\right)}}{{r_y}^2} + \frac{2}{{r_y}^2}. \tag{30}$$

Similarly, we can compute the remaining elements; subsequently, we obtain CRLB as follows:

$$\mathsf{Var}(\hat{r}_x) \geq \left[\mathbf{I}^{-1}(\boldsymbol{\theta})\right]_{11}, \quad \mathsf{Var}(\hat{r}_y) \geq \left[\mathbf{I}^{-1}(\boldsymbol{\theta})\right]_{22}. \tag{31}$$

When using only two measurements of range and bearing, we can obtain the lower bound, similarly. For example, $[\mathbf{I}(\theta)]_{11}$ can be obtained by removing the last two terms in (29). If CRLB for the distance estimation, i.e. $\sqrt{r_x^2 + r_y^2}$ is to be computed, we can use vector parameter CRLB for transformations, and is easily derived as follows [27]. If we define $\boldsymbol{\alpha} = h(\boldsymbol{\theta}) = \sqrt{r_x^2 + r_y^2}$, CRLB is derived as

$$\mathsf{Var}(\hat{\boldsymbol{\alpha}}) \geq \frac{\partial h(\boldsymbol{\theta})}{\partial \boldsymbol{\theta}} \mathbf{I}^{-1}(\boldsymbol{\theta}) \frac{\partial h(\boldsymbol{\theta})^{\top}}{\partial \boldsymbol{\theta}}, \tag{32}$$

where a Jacobian matrix $\frac{\partial h(\boldsymbol{\theta})}{\partial \boldsymbol{\theta}}$ is described as

$$\frac{\partial h(\boldsymbol{\theta})}{\partial \boldsymbol{\theta}} = \left[\frac{\partial h(\boldsymbol{\theta})}{\partial \theta_1} \quad \frac{\partial h(\boldsymbol{\theta})}{\partial \theta_2} \quad \cdots \quad \frac{\partial h(\boldsymbol{\theta})}{\partial \theta_L} \right] = \left[\frac{r_x}{\sqrt{r_x^2+r_y^2}} \quad \frac{r_y}{\sqrt{r_x^2+r_y^2}} \quad 0 \quad 0 \right] \tag{33}$$

FUNDING

This work was supported by the Basic Science Research Program through the National Research Foundation of Korea funded by the Ministry of Education (NRF-2016R1D1A1A09918304 & NRF-2019R1I1A1A01058976).

CONFLICT OF INTEREST

The authors declare no potential conflict of interests.

REFERENCES

[1] E. Bekir, "Adaptive kalman filter for tracking maneuvering targets," *Journal of Guidance, Control, and Dynamics*, vol. 6, no. 5, pp. 414–416, 1983.

[2] Y. Boers and J. Driessen, "Interacting multiple model particle filter," *IEE Proceedings-Radar, Sonar and Navigation*, vol. 150, no. 5, pp. 344–349, 2003.

[3] H.-W. Li and J. Wang, "Particle filter for manoeuvring target tracking via passive radar measurements with glint noise," *IET Radar, Sonar & Navigation*, vol. 6, no. 3, pp. 180–189, 2012.

[4] T. Zhang, S. Liu, C. Xu, B. Liu, and M.-H. Yang, "Correlation particle filter for visual tracking," *IEEE Transactions on Image Processing*, vol. 27, no. 6, pp. 2676–2687, 2018.

[5] P. Closas and A. Guillamon, "Sequential estimation of intrinsic activity and synaptic input in single neurons by particle filtering with optimal importance density," *EURASIP Journal on Advances in Signal Processing*, vol. 2017, no. 1, p. 65, 2017.

[6] P. Guarniero, A. M. Johansen, and A. Lee, "The iterated auxiliary particle filter," *Journal of the American Statistical Association*, pp. 1–12, 2017.

[7] A. Murangira, C. Musso, and K. Dahia, "A mixture regularized rao-blackwellized particle filter for terrain positioning," *IEEE Transactions on Aerospace and Electronic Systems*, vol. 52, no. 4, pp. 1967–1985, 2016.

[8] D. Fox, "Adapting the sample size in particle filters through KLD-sampling," *The international Journal of robotics research*, vol. 22, no. 12, pp. 985–1003, 2003.

[9] T. Li, S. Sun, and T. P. Sattar, "Adapting sample size in particle filters through KLD-resampling," *Electronics Letters*, vol. 49, no. 12, pp. 740–742, 2013.

[10] T. Zhou, D. Peng, C. Xu, W. Zhang, and J. Shen, "Adaptive particle filter based on Kullback–Leibler distance for underwater terrain aided navigation with multi-beam sonar," *IET Radar, Sonar & Navigation*, vol. 12, no. 4, pp. 433–441, 2018.

[11] J. H. Kotecha and P. M. Djuric, "Gaussian particle filtering," *IEEE Transactions on signal processing*, vol. 51, no. 10, pp. 2592–2601, 2003.

[12] J. Lim and D. Hong, "Gaussian particle filtering approach for carrier frequency offset estimation in ofdm systems," *IEEE Signal Processing Letters*, vol. 20, no. 4, pp. 367–370, 2013.

[13] J. Míguez, M. F. Bugallo, and P. M. Djurić, "A new class of particle filters for random dynamic systems with unknown statistics," *EURASIP Journal on Advances in Signal Processing*, vol. 2004, no. 15, pp. 1–17, 2004.

[14] J. Lim and D. Hong, "Cost reference particle filtering approach to high-bandwidth tilt estimation," *IEEE Transactions on Industrial Electronics*, vol. 57, no. 11, pp. 3830–3839, 2010.

[15] J. Lim, "Particle filtering for nonlinear dynamic state systems with unknown noise statistics," *Nonlinear Dynamics*, vol. 78, no. 2, pp. 1369–1388, 2014.

[16] M. Arulampalam, S. Maskell, N. Gordon, and T. Clapp, "A tutorial on particle filters for online nonlinear/non-Gaussian Bayesian tracking," *IEEE Trans. Signal Processing*, vol. 50, no. 2, Feb. 2002.

[17] F. Gustafsson, F. Gunnarsson, N. Bergman, U. Forssell, J. Jansson, R. Karlsson, and P.-J. Nordlund, "Particle filters for positioning, navigation, and tracking," *IEEE Transactions on signal processing*, vol. 50, no. 2, pp. 425–437, 2002.

[18] P. M. Djuric, M. Vemula, and M. F. Bugallo, "Target tracking by particle filtering in binary sensor networks," *IEEE Transactions on Signal Processing*, vol. 56, no. 6, pp. 2229–2238, 2008.

[19] J. Lim, "A target tracking based on bearing and range measurement with unknown noise statistics," *Journal of Electrical Engineering and Technology*, vol. 8, no. 6, pp. 1520–1529, 2013.

[20] X.-M. Shen and L. Deng, "Game theory approach to discrete h/sub/spl infin//filter design," *IEEE Transactions on Signal Processing*, vol. 45, no. 4, pp. 1092–1095, 1997.

[21] D. Simon, "A game theory approach to constrained minimax state estimation," *IEEE Transactions on Signal Processing*, vol. 54, no. 2, pp. 405–412, 2006.

[22] M. K. Pitt and N. Shephard, "Filtering via simulation: Auxiliary particle filters," *Journal of the American statistical association*, vol. 94, no. 446, pp. 590–599, 1999.

[23] J. Lim, "Performance degradation due to particle impoverishment in particle filtering," *Journal of Electrical Engineering & Technology*, vol. 9, no. 6, pp. 2107–2113, 2014.

[24] C. Musso, N. Oudjane, and F. Le Gland, "Improving regularised particle filters," in *Sequential Monte Carlo methods in practice*. Springer, 2001, pp. 247–271.

[25] S. Xu, "Particle filtering for systems with unknown noise probability distributions," Ph.D. dissertation, Department of Electrical and Computer Engineering, Stony Brook University-SUNY, Stony Brook, New York 11794, December 2006.

[26] X. R. Li, Z. Zhao, and V. P. Jilkov, "Practical measures and test for credibility of an estimator," in *Proc. Workshop on Estimation, Tracking, and Fusion?A Tribute to Yaakov Bar-Shalom*, 2001, pp. 481–495.

[27] S. M. Kay, *Fundamentals of statistical signal processing*. Prentice hall signal processing series, 1993, vol. 1, estimation Theory.